

Wave-Shape-Tolerant Photonic Quantum Gates


I. Babushkin^{1,2,3}, A. Demircan^{1,3}, M. Kues^{3,4}, and U. Morgner^{1,3}

¹*Institute of Quantum Optics, Leibniz University Hannover, Welfengarten 1, 30167 Hannover, Germany*

²*Max Born Institute, Max-Born-Strasse 2a, 12489 Berlin, Germany*

³*Cluster of Excellence PhoenixD (Photonics, Optics, and Engineering - Innovation Across Disciplines), Welfengarten 1, 30167 Hannover, Germany*

⁴*Institute of Photonics, Leibniz University Hannover, Nienburgerstrasse 17, 30519 Hannover, Germany*

 (Received 17 May 2021; revised 21 December 2021; accepted 13 January 2022; published 4 March 2022)

Photons, acting as “flying qubits” in propagation geometries such as waveguides, appear unavoidably in the form of wave packets (pulses). The actual shape of the photonic wave packet as well as possible temporal and spectral correlations between the photons play a critical role in successful scalable computation. Currently, unentangled indistinguishable photons are considered a suitable resource for scalable photonic circuits. Here we show that using so-called coherent photon conversion, it is possible to construct flying-qubit gates which are not only insensitive to wave shapes of the photons and temporal and spectral correlations between them but which also fully preserve these wave shapes and correlations upon the processing. This allows the use of photons with correlations and purity in a very broad range for a scalable computation. Moreover, such gates can process entangled photonic wave packets even more effectively than unentangled ones.

DOI: [10.1103/PhysRevLett.128.090502](https://doi.org/10.1103/PhysRevLett.128.090502)

Despite photons being seemingly ideal candidates for carrying quantum information, robust scalable gates and circuits for the photonic qubits remain yet illusive. The difficulty is that photons do not interact with each other directly, and thus either indirect interaction via a nonlinear medium [1–12] or “emulation” of interaction using measurements [13–16] are needed. The wave shapes either in time [17–21] or in frequency [22–24] (or both together [25]) may themselves represent qubits. Alternatively, information can be stored in degrees of freedom orthogonal to wave shapes, such as which path [15], polarization [15], field quadratures [26,27], or angular momentum [28]. In all cases, regardless of the used approach, the shape of the photonic wave packet is of primary importance for the gate action.

One ideally would desire a gate, working with (almost) arbitrary photonic wave shapes and fully preserve them during the computation—even if the wave shapes are not unentangled or not pure. We will call such gates “wave shape tolerant.” Formally speaking, wave shape tolerantness is a quite strong property; for instance, if we delay one of the two photons in a two-photon gate so that they do not overlap in time anymore, the wave-shape-tolerant gate should still work. Are such gates possible at all?

In linear optical circuits (LOCs) [13–16], which consist of linear interferometric networks and measurements of ancillary qubits, it is known [29,30] that for scalable operation the photons in different channels have to be independent and indistinguishable, so that no which-path information can be extracted, since its presence breaks the interference in linear optical elements, and introduces

incoherence during measurements [29–31]. Although the action of LOCs was recently extended to a more general class of states [31], they certainly are not wave shape tolerant in the sense mentioned above.

The situation seems even worse if we consider a recent proposal based on so-called coherent photon conversion (CPC), where the photon-photon interaction is based on a four-wave mixing (FWM) process in the presence of a strong coherent laser field [1]. This coherent field amplifies the action of the $\chi^{(3)}$ nonlinearity between the remaining three waves, which are in a Fock state. A two-photon wave packet sent to the input of a CPC device should experience up- and down-conversion cycles, attaining a nonlinear phase shift of π after each cycle, thus leading to a controlled-Z (CZ) gate functionality. Unfortunately, soon after the discovery of this approach it was noted [4] that, if the finite size of the wave packets is taken into account, it does not work, even if the participating photons are temporally unentangled and indistinguishable, since only the parts of the biphoton wave packet located at the same position in space (or time) can effectively interact. This problem can be, however, solved if the photons have nonzero group velocities relative to each other [2,5]. In this case, parts of the photons that were initially separated, eventually cross and can interact at that moment. This approach was very recently partially realized experimentally [8] in a system with electromagnetic-induced transparency, however, at the cost of partial loss of “working” photons. In addition, three-photon interaction was observed in cold Rydberg atoms [32].

Nevertheless, with or without a relative movement of the photonic wave packets, it seems at first sight that the CPC-based approach has no chances to produce wave-shape-tolerant gates, since, by up-conversion of a biphoton wave packet (described by a two-dimensional distribution) into a single photon (described by a one-dimensional waveform), some information about the initial two-photon wave shape is unavoidably lost, and the back-conversion cannot restore it anymore. Therefore, the final wave shape seemingly can coincide with the initial one only by chance.

Despite these objections, here we show that CPC-based gates can indeed possess the property of being wave shape tolerant, if the wave packet is slowly varying on the timescale of the effective photon-photon interaction, or, equivalently, if the suitable fourth-order coherence time is large enough. This implies also scalability of the gates to many entangled photons, as well as their ability to work with mixed states. Moreover, we show that processing of time- and frequency-entangled photons can be more efficient than that of the unentangled ones.

The model.—The CPC approach with group-velocity-unmatched pulses proposed in [2] is shown in Fig. 1. The photons in Fock states at frequencies ω_s , ω_i , and ω_a , which we call signal (*s*), idler (*i*), and ancilla (*a*), respectively, interact via the FWM process described by the susceptibility $\chi^{(3)} = \chi^{(3)}(\omega_a; \omega_p, \omega_s, \omega_i)$ in the presence of a strong coherent field (*p*) at frequency ω_p with the peak electric field E_p . This induces an effective three wave mixing interaction between the *a*, *s*, and *i* wave packets. Each of the wave packets is described by the frequency-dependent operators $a_a(\omega_a)$, $a_s(\omega_s)$, and $a_i(\omega_i)$.

Since only parts of the wave packets that are close to each other (in space or time) can interact, one has to resolve the finite size of the interaction region [2]. In the previous considerations [2,5], the Hamiltonian containing spatial nonlocality was used for this purpose, attracting, however,

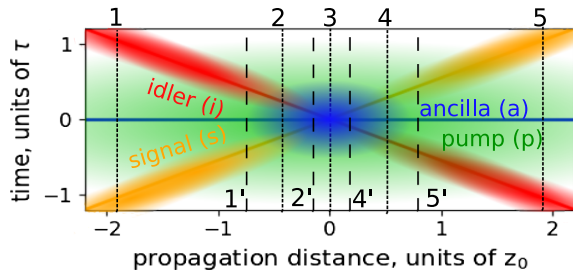


FIG. 1. CPC-based CZ gate with group-velocity-unmatched pulses. Single photon wave packets denoted as ancilla (*a*, blue), signal (*s*, orange), and idler (*i*, red) propagate in the field of a strong coherent pump (*p*, green), interacting via the FWM process. The moving centers of the wave packets are indicated by solid lines. Color change denotes schematically conversion of photons. Vertical lines and numbers correspond to the positions of the snapshots shown in Fig. 2 (lines labeled 1–5 refer to $S1$, $S2$, $S4$; lines labeled 1', 2', 3, 4', 5' refer to $S3$).

critics as physically nontransparent [5]. Here we operate, instead, in terms of noninstantaneous response, that is, with nonlocality in time rather than in space, which is more physically justified (see [33,34] and also below), leading nevertheless to a formulation rather equivalent to [2,5] in our particular case. The noninstantaneous interaction can be represented with a Hamiltonian

$$H = \hbar\gamma' \int \tilde{h}(\omega_a, \omega_s, \omega_i) a_s^\dagger(\omega_s) a_i^\dagger(\omega_i) a_a(\omega_a) \times d\omega_s d\omega_i d\omega_a + \text{H.c.} \quad (1)$$

Here \hbar is the Plank constant, $\gamma' \sim \chi^{(3)} E_p$ is the interaction strength [see more details below, after Eqs. (4) and (5)], and \tilde{h} describes the noninstantaneous response of the nonlinear medium in the frequency domain. Although our further analysis shows that the particular form of \tilde{h} is not important, for numerical simulations we use the function

$$\tilde{h}(\omega_a, \omega_s, \omega_i) = \frac{\delta(\omega_p - \omega_a + \omega_s + \omega_i)}{\sqrt{2\pi}} e^{-\sigma^2(\omega_s^2 + \omega_i^2)/2}, \quad (2)$$

where δ is the Dirac δ function. This response function has a transparent physical meaning: δ function ensures the energy conservation; the frequency-dependent form factor effectively “switches off” the interaction at frequencies much larger than $\omega_R \approx 2\pi/\sigma$. This represents schematically a typical frequency-dependent $\chi^{(3)}$ for dielectrics [33–35], which vanishes at frequencies far above the band gap. The presence of the cutoff frequency ω_R in Eq. (2) means that the photons effectively interact with each other only if they are separated in time by an interval smaller than σ . This implies also spatial nonlocality: the photons interact if they are at a distance smaller than $c\sigma$. For “typical” materials like fused silica σ has been recently measured to be at the level of hundreds of attoseconds [36,37].

Here we assume 1D propagation geometry, e.g., in waveguides, and consider a FWM-phase-matched evolution along the propagation axis, which we denote as z . The equation of motion in time t can be written in the form of the Schrödinger equation $i\hbar\partial_t|\Psi\rangle = (H_0 + H)|\Psi\rangle$, where H_0 is the non-interacting Hamiltonian. We restrict our consideration to $n \leq 1$ photons in *s*, *i*, or *a* channels (and strictly zero number of photons in *a* at the input) and formulate the corresponding wave vector $|\Psi\rangle$ in terms of temporal modes [19],

$$|\Psi\rangle = \int \int \Psi_{si}(t_s, t_i, z) |t_s\rangle_s |t_i\rangle_i dt_s dt_i + \sum_l \left(\int \Psi_l(t_l, z) |t_l\rangle_l dt_l \right) + |000\rangle, \quad (3)$$

where $l = \{s, i, a\}$, $|t_j\rangle_j = \int e^{it_j\omega_j} a_j^\dagger(\omega_j) |0\rangle_{\omega_j} d\omega_j$, $j = \{s, i\}$, and $|t_a\rangle_a = \int e^{it_a(\omega_a - \omega_p)} a_a^\dagger(\omega_a) |0_{\omega_a}\rangle_a d\omega_a$, where a^\dagger and $|0_{\omega_j}\rangle_j$ denote creation operators and vacuum states for the corresponding modes and frequencies, whereas $|000\rangle$

denotes the vacuum in s , i , and a channels. A wave-shape-tolerant CZ operation on the photons in s and i channels $\alpha_{00}|00\rangle + \alpha_{01}|01\rangle + \alpha_{10}|10\rangle + \alpha_{11}|11\rangle \rightarrow \alpha_{00}|00\rangle + \alpha_{01}|01\rangle + \alpha_{10}|10\rangle - \alpha_{11}|11\rangle$ for arbitrary coefficients α_{ij} is expressed as $\Psi_{si}(t_s, t_i) \rightarrow -\Psi_{si}(t_s, t_i)$, $\Psi_j(t_j) \rightarrow \Psi_j(t_j)$, $|000\rangle \rightarrow |000\rangle$; that is, all photonic wave shapes should remain invariant, whereas the sign flip takes place by the two-photon wave packet only. If the input photons are (nearly) indistinguishable, this might be also considered as the nonlinear sign (NS) gate.

Assuming absence of the higher-order linear dispersion terms, that is, $H_0 = \sum_j \hbar \int \omega a_j^\dagger(\omega) a_j(\omega) d\omega + \text{H.c.}$, allows one to write down the evolution equations for the wave shapes along the z direction in the frame of reference propagating with the group velocity of the ancilla v_a (note that t and z formulations are mathematically equivalent in our case [38] as described in the Supplemental Material [39], which includes Refs. [40–59]),

$$\frac{\partial \Psi_{si}(t_s, t_i, z)}{\partial z} = -\beta_{1s} \frac{\partial \Psi_{si}(t_s, t_i, z)}{\partial t_s} - \beta_{1i} \frac{\partial \Psi_{si}(t_s, t_i, z)}{\partial t_i} - i\gamma \int h(t_a, t_s, t_i) \Psi_a(t_a, z) dt_a, \quad (4)$$

$$\frac{\partial |000\rangle}{\partial z} = 0,$$

$$\frac{\partial \Psi_a(t_a, z)}{\partial z} = -i\gamma \int \int h(t_a, t_s, t_i) \Psi_{si}(t_s, t_i, z) dt_s dt_i, \quad (5)$$

$$\frac{\partial \Psi_m(t_j, z)}{\partial z} = -\beta_{1m} \frac{\partial \Psi_m(t_m, z)}{\partial t_m}.$$

Here $m = \{s, i\}$, $\beta_{1j} = 1/v_j - 1/v_a$ ($j = \{s, i, a\}$), v_j are the corresponding group velocities, $h(t_a, t_s, t_i)$ is the Fourier transform of $\tilde{h}(\omega_a, \omega_s, \omega_i)$ with the phase coefficients moved to wave shapes in Eq. (3):

$$h(t_a, t_s, t_i) = \frac{1}{2\pi\sigma^2} e^{-(t_s-t_a)^2/2\sigma^2} e^{-(t_i-t_a)^2/2\sigma^2}. \quad (6)$$

$\gamma \approx \gamma'/v_a$ can be obtained from the limit of instantaneous nonlinearity [40] (see details in the Supplemental Material [39]) as $\gamma = \hbar\omega_p^2 n_2 \Phi_p / cS$, where S is the effective area of the beam (assumed to be the same for all waves), c is the

speed of light in vacuum, $\Phi_p = \sqrt{SI_p/n_p^2 \hbar\omega_p}$ is the square root of the number of pump photons per unit time, I_p is the intensity of the pump p , n_2 is the nonlinear refractive index corresponding to $\chi^{(3)}$ of the relevant FWM process, and n_p is the refractive index for the pump wavelength.

We assume furthermore $\beta_{1s} = -\beta_{1i} \equiv \beta_1$; that is, the signal and idler pulses propagate with equal velocities of the opposite sign in the frame of reference of the ancilla (see Fig. 1). The parts of Eqs. (4) and (5) corresponding to different input photon numbers in s and i channels are uncoupled and thus can be considered separately. The states with zero or one input photons contain no interaction and allow an analytical solution: the vacuum state remains unchanged, whereas the single-photon wave packets $\Psi_j(t_j, z)$, $j = \{s, i\}$ are translated with no change of shape or phase from the beginning to the end of the waveguide. In contrast, the two-photon amplitude requires more involved consideration.

Two-photon wave shapes: Numerical simulations.—If we denote the initial pulse duration by τ , the effective overlap (and thus interaction) of the signal and idler wave shapes takes place over the distance $\approx z_0$, where $z_0 = \tau/\beta_1$. For the sake of generality, we normalized time t to τ and z to z_0 , leading to the following renormalizations in Eqs. (4) and (5): $\beta_{1j} \rightarrow 1$ for $j = \{s, i\}$, $\gamma \rightarrow \gamma\beta_1/\sqrt{\tau}$, $h \rightarrow h/\tau^2$, $\Psi_a \rightarrow \Psi_a/\sqrt{\tau}$, $\Psi_{si} \rightarrow \Psi_{si}/\tau$. Numerical simulations were made in the range $z = [-L/2, L/2]$ for $L = 4.4z_0$ (see Fig. 1). We initialized our wave shapes at $z = -L/2$ with the vacuum for the ancilla ($\Psi_a = 0$) and two photons in signal and idler modes with various initial distributions $\Psi_{si}(t_s, t_i, -L/2) = \Psi^{(\text{in})}(t_s, t_i)$ for four different simulations denoted as S1–S4 in Fig. 2. For the simulations S1–S4 we used the wave shape

$$\Psi^{(\text{in})}(t_s, t_i) = \Psi_0 \mathcal{R}_\theta \left[\text{sech} \left(\frac{t_s - t_{s0}}{\tau_s} \right) \text{sech} \left(\frac{t_i - t_{i0}}{\tau_i} \right) e^{i\phi} \right],$$

where Ψ_0 is a normalization factor leading to $\|\Psi_{si}(t_s, t_i, -L/2)\| = 1$ [here $\|f\|$ is the norm of a function f : $\|f\| = \int \int f(x, y) dx dy$], \mathcal{R}_θ is the transformation rotating $\Psi(t_s, t_i)$ in (t_s, t_i) plane by the angle θ , and $\phi = \phi(t_s, t_i)$ describes an additional time-dependent phase. For S1 we

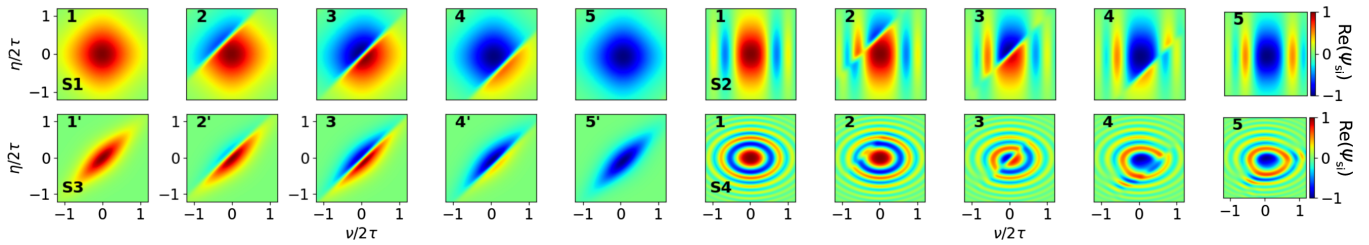


FIG. 2. Snapshots of the signal idler wave packet represented by $\text{Re}(\Psi_{si}(t_s, t_i, z))$ for different initial wave shapes marked as S1–S4 (see text) shown in the moving coordinates $\eta = (t_s - z\beta_{1s})$, $\nu = (t_i - z\beta_{1i})$. The positions of the snapshots in z are indicated in Fig. 1 by the vertical lines and corresponding numbers. Sign flip of $\text{Re}(\Psi_{si})$ indicates the successful CZ gate operation. The wave shapes in S1–S3 are conserved, which is not the case for S4 where distortions appear.

used (in normalized units mentioned above) $\tau_s = \tau_i = 1$, $\phi = 0$, $\theta = 0$, which gives a separable wave shape; $t_{s0} = -1.2\tau_s$, and $t_{s0} = 1.2\tau_s$. For S2, in comparison to S1, we introduced a (moderate) chirp into the idler $\phi = Ct_i^2$, $C = 1.82/\tau^2$; the wave shape becomes more complicated but yet fully separable. For S3 we assumed $\phi = 0$ but different signal and idler durations: $\tau_s = 1$, $\tau_i = 1/3$, and $\theta = -\pi/4$, constructing thereby a state with signal and idler being entangled. Finally, in S4, in comparison to S1, we introduced extremely fast phase oscillations by taking $\phi = iC_s t_s^2 + iC_i t_i^2$ with $C_s = C_i/2 = 10/\tau^2$.

In all simulations, we used $\sigma/\tau = 0.05$. As a ‘‘reference case’’ we may take a fused silica waveguide with $n_p = 1.45$, $n_2 = 3 \times 10^{-16} \text{ cm}^2/\text{W}$ and $S = 1 \mu\text{m}^2$. We also assume σ of 500 as, which is of the order of values measured recently [36,37]. The normalized parameters mentioned above correspond then to $I_p = 20 \text{ TW}/\text{cm}^2$ and FWHM duration of 10 fs ($\tau = 5.4 \text{ fs}$). The interaction distance is then on the kilometer range: taking $z_0 = 6.26 \text{ km}$ ($\beta_1 = 0.86 \text{ fs}/\text{km}$) leads to the fidelity $\mathcal{F} = 99.7\%$ for S1 (see definition of \mathcal{F} below). On the other hand, faster than the optimal propagation speed reduces back-conversion and thus fidelity; for instance, increasing β_1 2 times leads to $\mathcal{F} = 90\%$. We note, furthermore, that the gate length is inversely proportional to n_2/S ; using novel photonic materials [44–49], such as silicon, nanocrystalline diamond, and others may reduce the gate length to a centimeter range. For further discussion of these issues, see the Supplemental Material [39].

The results of simulations are shown in Fig. 2 as snapshots of $\text{Re}\Psi_{si}(t_s, t_i, z)$ at the positions marked by 1–5 (for S1–S3) and 1', 2', 3, 4', 5' (for S3) in Fig. 1 by vertical lines. A successful gate operation assumes the phase change of π , which means the sign flip of $\text{Re}\Psi_{si}(t_s, t_i, z)$. As one can see in Fig. 2, the gate operation takes place in a form of a ‘‘front’’ of the size $\sim\sigma$ which moves through the wave shape. In the case S3 the interaction is completed at around 3 times shorter distance due to the 3 times smaller duration of the wave packet in the direction of the front movement.

Interestingly, at the point ‘‘3’’ we have a Bell-type state $|+\rangle_s|+\rangle_i - |-\rangle_s|-\rangle_i$, where $|\pm\rangle_j$ denotes the signal ($j = s$) or idler ($j = i$) photon, located in upper-left (+) or lower-right (–) corner of the (ν, η) plain.

Another important case is the presence of temporal offsets $[\Psi_{si}(t_s, t_i) \rightarrow \Psi_{si}(t_i + \tau_i, t_s + \tau_s)]$ for some small τ_s, τ_i . They also can be processed in the fully wave-shape-tolerant way (not shown in Fig. 2, see Supplemental Material [39] for more details on this).

The quality of the gate operation and its ability to keep the wave shape can be quantified by the fidelity \mathcal{F} presented in Fig. 3 and defined as $\mathcal{F}(z) = \frac{1}{2}|1 - \int \int \Psi_{si}^{(\text{norm})}(t_s, t_i, z) \Psi_{si}^{(\text{norm})*}(t_s, t_i) dt_s dt_i|$, where $\Psi_{si}^{(\text{norm})}(t_s, t_i, z) = \Psi_{si}(t_s, t_i, z) / \|\Psi_{si}(t_s, t_i, z)\|$. $\mathcal{F} = 1$ corresponds to a perfect gate operation, including full conservation of the pulse shape.

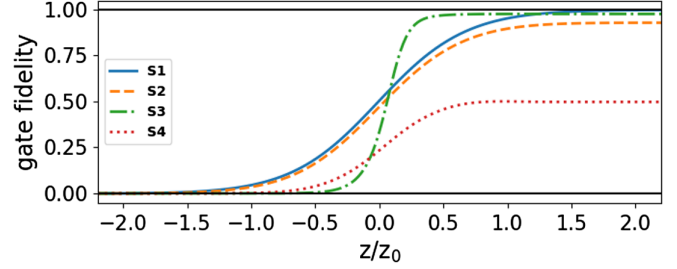


FIG. 3. Evolution of the gate fidelity $\mathcal{F}(z)$ for the simulations S1–S4 in Fig. 2.

One can see indeed from Figs. 2 and 3, that for the cases S1–S3 not only is the phase successfully flipped, but the wave shape also remains intact after the gate. On the other hand, the phase deformation introduced in S4 makes the wave shape change quickly on the scale of σ , leading to a visibly corrupted final wave shape reflected in the low fidelity in Fig. 3.

Summarizing, smooth enough wave packets are processed in a wave-shape-tolerant way. On the other side, processing of wave shapes with features, ‘‘sharp’’ on the scale of σ , is not anymore perfect.

Two-photon wave shapes: Analytics.—We proceed further with a more general analytical insight into the dynamics of two-photon wave shapes. We derive the equation describing evolution of the wave packet Ψ_{si} for an arbitrary response function h localized mostly in the region of the size $\approx\sigma \times \sigma$ of the point $t_s = t_i$ and being symmetric in respect to its maxima (h used above is a particular example of such function), whereas Ψ_{si} is slow on the scale of σ , meaning

$$|\partial_{t_j} \Psi_{si}(t_s, t_i, z)| \ll |\Psi_{si}(t_s, t_i, z)|/\sigma \quad (7)$$

for $j = \{s, i\}$ for all t_s and t_i . Under these conditions, the equation governing the evolution of a small part $\delta\Psi$ of the size $\sigma \times \sigma$ of the whole wave packet Ψ_{si} is described by (see Supplemental Material [39] for more details)

$$\partial_{\xi\xi} \delta\Psi(\xi, \eta, \nu) + \frac{\gamma^2}{\sigma} K(\xi - \xi_0) \delta\Psi(\xi, \eta, \nu) = 0, \quad (8)$$

where $\xi = \beta_1(z - t_i/\beta_{1i} + t_s/\beta_{1s})$, $\eta = (t_s - z\beta_{1s})$, $\nu = (t_i - z\beta_{1i})$, and $K(\xi - \xi_0)$ is a coupling factor that is of the order of 1 close to $\xi = \xi_0$ and quickly approaches zero as $|\xi - \xi_0|$ becomes larger than σ (that is, if we leave the σ vicinity of ξ_0). For instance, for h given by Eq. (6) we have $K(\xi - \xi_0) \propto \exp[-(\xi - \xi_0)^2/4\sigma^2]$.

Equation (8) is an equation for a harmonic oscillator with variable frequency. In the interaction region of the size σ near $\xi = \xi_0$, the harmonic oscillator (and thus the conversion) is effectively switched on whereas outside of the region it is off. This region defines the conversion front visible in Fig. 2. For the perfect gate operation, exactly half of an oscillation period is necessary. Since Eq. (8) is linear

and the evolution starts from the same initial phase (Ψ_{si} is at maximum) in all points (η, ν) , the same part of the oscillation is performed everywhere, making the shape of Ψ_{si} preserved.

Importantly, this result is general in the sense that it applies for any Ψ_{si} satisfying the slowness condition (7), also for an arbitrary noninstantaneous response h satisfying the conditions mentioned above. $S4$ in Fig. 2 shows that, if the condition (7) is not satisfied, the gate may indeed modify the wave packet shape, since the noninstantaneous interaction mixes different pieces of the wave shape.

Operation for mixed states.—Here we show that the CZ gate works properly for mixed states (described by a density matrix ρ_{si}) if a more general slowness condition is satisfied. We sketch the consideration, and technical details can be found in the Supplemental Material [39]. ρ_{si} can always be represented as a pure state $|\Psi\rangle$ in some “larger” space [60]. In our case, $|\Psi\rangle$ can be represented as a sum of orthogonal contributions with amplitudes given by a set of “partial wave shapes” $\Psi_{si}^{\{w\}}(t_s, t_i)$, describing the signal-idler state in each of the configurations $\{w\}$ of the rest of that larger space. Every $\Psi_{si}^{\{w\}}$ evolves fully independently from the others and obeys the same Schrödinger equation [Eqs. (4) and (5)]. Therefore, ρ_{si} will be processed correctly if all of $\Psi_{si}^{\{w\}}$ satisfy the slowness condition (7).

Using the fourth-order coherence function $\Gamma^{(2,2)}$ [61]

$$\Gamma^{(2,2)}(\tau_s, \tau_i) = \text{tr}[\rho_{si} a_s^\dagger(t_s - \tau_s) a_i^\dagger(t_i - \tau_i) a_s(t_s) a_i(t_i)],$$

Equation (7) can be reformulated in an equivalent form as

$$\Gamma^{(2,2)}(\tau_s, \tau_i) \approx \Gamma^{(2,2)}(0, 0) \quad (9)$$

for $|\tau_s| \lesssim \sigma$ and $|\tau_i| \lesssim \sigma$. Equation (9) is applicable for density matrices. It obviously cannot be satisfied if $\mathcal{T}^{(4)} \lesssim \sigma$, where $\mathcal{T}^{(4)}$ is the coherence time defined as the width of $\Gamma^{(2,2)}(\tau_s, \tau_i)$, so the opposite condition

$$\mathcal{T}^{(4)} \gg \sigma \quad (10)$$

is therefore necessary for the validity of Eq. (9). Except for some pathological wave shapes, $\Gamma^{(2,2)}$ decreases monotonously near the origin $(\tau_s, \tau_i) = (0, 0)$. Thus, in most cases, Eq. (10) delivers also the sufficient condition and can be therefore considered as a suitable slowness criterion.

Discussion and conclusions.—We showed that CPC-based gates can be wave shape tolerant, that is, successfully process arbitrary wave shapes keeping them intact, if the wave shapes vary slowly on the timescale of σ , the noninstantaneous response time of the nonlinearity. This condition can be reformulated in the form of a constraint [(9) or (10)] on the fourth-order coherence, which is also applicable to mixed states. It is a very strong property: most wave shapes are changing slowly on the scale of the optical

wavelength λ and thus on the scale of σ , since most typically $\sigma \leq \lambda$ or even $\sigma \ll \lambda$ in optics. The smallest σ appear for off-resonant nonlinearities, such as in fused silica at optical frequencies, in which case it lies in the attosecond range [36,37]. Our simulations indicate that in this situation the successful gate operation is realizable if the strong coherent pump in the TW/cm² range and the pulse durations in the femtosecond range are used.

Wave shape tolerantness relaxes significantly the requirements to the photon sources needed for scalable computing. The photons do not need to be indistinguishable, unentangled, or even pure anymore. Moreover, as we have seen, some entangled distributions promise a significant advantage in the resulting gate size over uncorrelated photons.

I. B. and U. M. thank Deutsche Forschungsgemeinschaft (DFG, German Research Foundation), Projects No. BA 4156/4-2 and No. MO 850-19/2 for support. I. B., A. D., M. K., and U. M. acknowledge support from Germany’s Excellence Strategy within the Cluster of Excellence EXC 2122 PhoenixD (Project ID No. 390833453) and Germany’s Excellence Strategy EXC-2123 QuantumFrontiers (Project ID No. 390837967). M. K. acknowledges support from the German Ministry of Education and Research (PQuMAL project).

-
- [1] N. K. Langford, S. Ramelow, R. Prevedel, W. J. Munro, G. J. Milburn, and A. Zeilinger, Efficient quantum computing using coherent photon conversion, *Nature (London)* **478**, 360 (2011).
 - [2] K. Xia, M. Johnsson, P. L. Knight, and J. Twamley, Cavity-Free Scheme for Nondestructive Detection of a Single Optical Photon, *Phys. Rev. Lett.* **116**, 023601 (2016).
 - [3] M. Y. Niu, I. L. Chuang, and J. H. Shapiro, Qudit-Basis Universal Quantum Computation Using $\chi^{(2)}$ Interactions, *Phys. Rev. Lett.* **120**, 160502 (2018).
 - [4] B. Viswanathan and J. Gea-Banacloche, Multimode analysis of a conditional phase gate based on second-order nonlinearity, *Phys. Rev. A* **92**, 042330 (2015).
 - [5] B. Viswanathan and J. Gea-Banacloche, Analytical results for a conditional phase shift between single-photon pulses in a nonlocal nonlinear medium, *Phys. Rev. A* **97**, 032314 (2018).
 - [6] M. Kounalakis, C. Dickel, A. Bruno, N. K. Langford, and G. A. Steele, Tuneable hopping and nonlinear cross-Kerr interactions in a high-coherence superconducting circuit, *npj Quantum Inf.* **4**, 38 (2018).
 - [7] D. Tiarks, S. Schmidt-Eberle, T. Stolz, G. Rempe, and S. Dürr, A photon-photon quantum gate based on Rydberg interactions, *Nat. Phys.* **15**, 124 (2019).
 - [8] S. Sagona-Stopfel, R. Shahrokhshahi, B. Jordaan, M. Namazi, and E. Figueroa, Conditional π -Phase Shift of Single-Photon-Level Pulses at Room Temperature, *Phys. Rev. Lett.* **125**, 243601 (2020).

- [9] M. Heuck, K. Jacobs, and D. R. Englund, Controlled-Phase Gate Using Dynamically Coupled Cavities and Optical Nonlinearities, *Phys. Rev. Lett.* **124**, 160501 (2020).
- [10] A. Dot, E. Meyer-Scott, R. Ahmad, M. Rochette, and T. Jennewein, Converting one photon into two via four-wave mixing in optical fibers, *Phys. Rev. A* **90**, 043808 (2014).
- [11] E. Meyer-Scott, A. Dot, R. Ahmad, L. Li, M. Rochette, and T. Jennewein, Power-efficient production of photon pairs in a tapered chalcogenide microwire, *Appl. Phys. Lett.* **106**, 081111 (2015).
- [12] A. S. Solntsev, S. V. Batalov, N. K. Langford, and A. A. Sukhorukov, Complete conversion between one and two photons in nonlinear waveguides with tailored dispersion, [arXiv:2110.03110](https://arxiv.org/abs/2110.03110).
- [13] E. Knill, R. Laflamme, and G. J. Milburn, A scheme for efficient quantum computation with linear optics, *Nature (London)* **409**, 46 (2001).
- [14] J. L. O'Brien, G. J. Pryde, A. G. White, T. C. Ralph, and D. Branning, Demonstration of an all-optical quantum controlled-not gate, *Nature (London)* **426**, 264 (2003).
- [15] P. Kok, W. J. Munro, K. Nemoto, T. C. Ralph, J. P. Dowling, and G. J. Milburn, Linear optical quantum computing with photonic qubits, *Rev. Mod. Phys.* **79**, 135 (2007).
- [16] J. Carolan, C. Harrold, C. Sparrow, E. Martín-López, N. J. Russell, J. W. Silverstone, P. J. Shadbolt, N. Matsuda, M. Oguma, M. Itoh, G. D. Marshall, M. G. Thompson, J. C. F. Matthews, T. Hashimoto, J. L. O'Brien, and A. Laing, Universal linear optics, *Science* **349**, 711 (2015).
- [17] I. Marcikic, H. de Riedmatten, W. Tittel, V. Scarani, H. Zbinden, and N. Gisin, Time-bin entangled qubits for quantum communication created by femtosecond pulses, *Phys. Rev. A* **66**, 062308 (2002).
- [18] C. Xiong, X. Zhang, A. Mahendra, J. He, D.-Y. Choi, C. J. Chae, D. Marpaung, A. Leinse, R. G. Heideman, M. Hoekman, C. G. H. Roeloffzen, R. M. Oldenbeuving, P. W. L. van Dijk, C. Taddei, P. H. W. Leong, and B. J. Eggleton, Compact and reconfigurable silicon nitride time-bin entanglement circuit, *Optica* **2**, 724 (2015).
- [19] B. Brecht, D. V. Reddy, C. Silberhorn, and M. G. Raymer, Photon Temporal Modes: A Complete Framework for Quantum Information Science, *Phys. Rev. X* **5**, 041017 (2015).
- [20] V. Ansari, J. M. Donohue, B. Brecht, and C. Silberhorn, Tailoring nonlinear processes for quantum optics with pulsed temporal-mode encodings, *Optica* **5**, 534 (2018).
- [21] K.-H. Luo, S. Brauner, C. Eigner, P. R. Sharapova, R. Ricken, T. Meier, H. Herrmann, and C. Silberhorn, Nonlinear integrated quantum electro-optic circuits, *Sci. Adv.* **5**, eaat1451 (2019).
- [22] S. Ramelow, L. Ratschbacher, A. Fedrizzi, N. K. Langford, and A. Zeilinger, Discrete Tunable Color Entanglement, *Phys. Rev. Lett.* **103**, 253601 (2009).
- [23] L. Olislager, J. Cussey, A. T. Nguyen, P. Emplit, S. Massar, J.-M. Merolla, and K. P. Huy, Frequency-bin entangled photons, *Phys. Rev. A* **82**, 013804 (2010).
- [24] C. Reimer, M. Kues, P. Roztocky, B. Wetzel, F. Grazioso, B. E. Little, S. T. Chu, T. Johnston, Y. Bromberg, L. Caspani, D. J. Moss, and R. Morandotti, Generation of multiphoton entangled quantum states by means of integrated frequency combs, *Science* **351**, 1176 (2016).
- [25] M. Kues, C. Reimer, P. Roztocky, L. R. Cortés, S. Sciara, B. Wetzel, Y. Zhang, A. Cino, S. T. Chu, B. E. Little *et al.*, On-chip generation of high-dimensional entangled quantum states and their coherent control, *Nature (London)* **546**, 622 (2017).
- [26] S. L. Braunstein and P. van Loock, Quantum information with continuous variables, *Rev. Mod. Phys.* **77**, 513 (2005).
- [27] U. Andersen, G. Leuchs, and C. Silberhorn, Continuous-variable quantum information processing, *Laser Photonics Rev.* **4**, 337 (2010).
- [28] A. Mair, A. Vaziri, G. Weihs, and A. Zeilinger, Entanglement of the orbital angular momentum states of photons, *Nature (London)* **412**, 313 (2001).
- [29] A. B. U'ren, K. Banaszek, and I. A. Walmsley, Photon engineering for quantum information processing, *Quantum Inf. Comput.* **3**, 480, 23 (2003).
- [30] A. U'Ren, C. Silberhorn, K. Banaszek, I. Walmsley, R. Erdmann, W. Grice, and M. Raymer, Generation of pure-state single-photon wavepackets by conditional preparation based on spontaneous parametric downconversion, *Laser Phys.* **15**, 146 (2005).
- [31] I. Babushkin, U. Morgner, and A. Demircan, Stability of quantum linear logic circuits against perturbations, *J. Phys. A* **53**, 445307 (2020).
- [32] Q.-Y. Liang, A. V. Venkatramani, S. H. Cantu, T. L. Nicholson, M. J. Gullans, A. V. Gorshkov, J. D. Thompson, C. Chin, M. D. Lukin, and V. Vuletić, Observation of three-photon bound states in a quantum nonlinear medium, *Science* **359**, 783 (2018).
- [33] R. Boyd and M. Boyd, *Nonlinear Optics* (Academic Press, New York, 1992).
- [34] N. Bloembergen, *Nonlinear Optics* (World Scientific, Singapore, 1996).
- [35] C. Brée, *Nonlinear Optics in the Filamentation Regime* (Springer Science & Business Media, New York, 2012).
- [36] M. Hofmann, J. Hyyti, S. Birkholz, M. Bock, S. K. Das, R. Grunwald, M. Hoffmann, T. Nagy, A. Demircan, M. Jupé, D. Ristau, U. Morgner, C. Brée, M. Woerner, T. Elsaesser, and G. Steinmeyer, Noninstantaneous polarization dynamics in dielectric media, *Optica* **2**, 151 (2015).
- [37] A. Sommer, E. Bothschafter, S. Sato, C. Jakubeit, T. Latka, O. Razskazovskaya, H. Fattahi, M. Jobst, W. Schweinberger, V. Shirvanyan *et al.*, Attosecond nonlinear polarization and light-matter energy transfer in solids, *Nature (London)* **534**, 86 (2016).
- [38] N. Quesada, G. Triginer, M. D. Vidrighin, and J. E. Sipe, Theory of high-gain twin-beam generation in waveguides: From Maxwell's equations to efficient simulation, *Phys. Rev. A* **102**, 033519 (2020).
- [39] See Supplemental Material at <http://link.aps.org/supplemental/10.1103/PhysRevLett.128.090502> for derivation of equations, scalings, and analysis of stability against perturbations, which includes Refs. [40–59].
- [40] P. D. Drummond and M. Hillery, *The Quantum Theory of Nonlinear Optics* (Cambridge University Press, Cambridge, England, 2014).
- [41] J. D. Jackson, *Classical Electrodynamics* (John Wiley & Sons, Inc., New York, 1962).
- [42] I. Babushkin and L. Bergé, The fundamental solution of the unidirectional pulse propagation equation, *J. Math. Phys. (N.Y.)* **55**, 032903 (2014).

- [43] J. B. Conway, *A Course in Functional Analysis*, Graduate Texts in Mathematics (Springer, New York, 1994).
- [44] G. P. Agrawal, *Nonlinear Fiber Optics*, 5th ed. (Elsevier, New York, 2007).
- [45] J. Leuthold, C. Koos, and W. Freude, Nonlinear silicon photonics, *Nat. Photonics* **4**, 535 (2010).
- [46] M. Motojima, T. Suzuki, H. Shigekawa, Y. Kainuma, T. An, and M. Hase, Giant nonlinear optical effects induced by nitrogen-vacancy centers in diamond crystals, *Opt. Express* **27**, 32217 (2019).
- [47] F. Trojánek, K. Židek, B. Dzurňák, M. Kozák, and P. Malý, Nonlinear optical properties of nanocrystalline diamond, *Opt. Express* **18**, 1349 (2010).
- [48] T. Michinobu, J. C. May, J. H. Lim, C. Boudon, J.-P. Gisselbrecht, P. Seiler, M. Gross, I. Biaggio, and F. Diederich, A new class of organic donor–acceptor molecules with large third-order optical nonlinearities, *Chem. Commun.* **6**, 737 (2005).
- [49] B. Esembeson, M. L. Scimeca, T. Michinobu, F. Diederich, and I. Biaggio, A high-optical quality supramolecular assembly for third-order integrated nonlinear optics, *Adv. Mater.* **20**, 4584 (2008).
- [50] Y. P. Deng, X. H. Xie, H. Xiong, Y. X. Leng, C. F. Cheng, H. H. Lu, R. X. Li, and Z. Z. Xu, Optical breakdown for silica and silicon with double femtosecond laser pulses, *Opt. Express* **13**, 3096 (2005).
- [51] M. A. Tran, D. Huang, T. Komljenovic, J. Peters, A. Malik, and J. E. Bowers, Ultra-low-loss silicon waveguides for heterogeneously integrated silicon/III-V photonics, *Appl. Sci.* **8**, 1139 (2018).
- [52] M. A. Green, Improved silicon optical parameters at 25C, 295K and 300Kw including temperature coefficients, *Prog. Photovoltaics* **30**, 164 (2022).
- [53] C. M. Dietrich, I. Babushkin, J. R. Cardoso de Andrade, H. Rao, A. Demircan, and U. Morgner, Higher-order dispersion and the spectral behavior in a doubly resonant optical parametric oscillator, *Opt. Lett.* **45**, 5644–5647 (2020).
- [54] L. Zhang, Q. Lin, Y. Yue, Y. Yan, R. G. Beausoleil, and A. E. Willner, Silicon waveguide with four zero-dispersion wavelengths and its application in on-chip octave-spanning supercontinuum generation, *Opt. Express* **20**, 1685 (2012).
- [55] S. Roy and F. Biancalana, Formation of quartic solitons and a localized continuum in silicon-based slot waveguides, *Phys. Rev. A* **87**, 025801 (2013).
- [56] B. Debord, F. Amrani, L. Vincetti, F. Gérôme, and F. Benabid, Hollow-core fiber technology: The rising of gas photonics, *Fibers* **7**, 16 (2019).
- [57] A. Ferrando, E. Silvestre, J. J. Miret, and P. Andrés, Nearly zero ultraflattened dispersion in photonic crystal fibers, *Opt. Lett.* **25**, 790 (2000).
- [58] Y. Guo, Z. Jafari, L. Xu, C. Bao, P. Liao, G. Li, A. M. Agarwal, L. C. Kimerling, J. Michel, A. E. Willner *et al.*, Ultra-flat dispersion in an integrated waveguide with five and six zero-dispersion wavelengths for mid-infrared photonics, *Photonics Res.* **7**, 1279 (2019).
- [59] A. Mishra and R. Pant, Deep UV to NIR frequency combs via cascaded harmonic generation in a silica nanowire using nanojoule pulse energies, *Optica* **8**, 1210 (2021).
- [60] M. Nielsen and I. Chuang, *Quantum Computation and Quantum Information: 10th Anniversary Edition* (Cambridge University Press, Cambridge, England, 2010).
- [61] L. Mandel and E. Wolf, *Optical Coherence and Quantum Optics* (Cambridge University Press, Cambridge, England, 1995).